ELSEVIER

International Journal of Mass Spectrometry 205 (2001) 137–148

International Journal of Mass Spectrometry

Dissociative electron attachment in highly polar molecules: sodium halides

J.-P. Ziesel[a,*], R. Azria[b], D. Teillet-Billy[b]

[a]*Laboratoire Collisions Agrégats Réactivité, Université Paul Sabatier, 31062 Toulouse CEDEX, France*
[b]*Laboratoire des Collisions Atomiques et Moléculaires, Université Paris-Sud, 91405 Orsay CEDEX, France*

Received 13 March 2000; accepted 20 June 2000

Abstract

We have studied dissociative electron attachment in beams of the highly polar sodium halides. The only ions formed in NaX are Na^-, as halogen ions X^- are formed by attachment on the dimer $(NaX)_2$. The Na^- angular distributions show a strong asymmetry with respect to the 90° scattering angle, which is interpreted as an effect of the dipolar interaction in the attachment. We have attempted to determine the symmetry of the dissociative anion states by theoretical analysis of the experimental angular data. The Σ symmetry contributes only at energies close to the onsets, while the Π symmetry is dominant over most of the processes. (Int J Mass Spectrom 205 (2001) 137–148) © 2001 Elsevier Science B.V.

Keywords: Sodium halides; Dissociative electron attachment; Anion state symmetry

1. Introduction

The interaction of electrons with polar molecules has received renewed interest as a consequence of the scattering features observed in the hydrogen halides [1–5] and of the developments in chemical lasers and magnetohydrodynamics. Unlike the hydrogen halides, the anion ground state $X^1\Sigma^+$ of the highly polar alkali halides is bound and has been described as the neutral alkali atom polarized by the halide negative ion [6 and references therein]. The first evidence of a bound state came from a photodetachment experiment in LiCl [7] in which the binding energy of 0.61 eV was in good agreement with the calculated value [8]. Vertical electron affinities have been further determined in other alkali halides, both experimentally [6] and theoretically [9]. Because of their large dipole moment well above the critical value (~2.5 D), dipole-bound states should exist in addition to the valence anion state [10]. Complementary to photodetachment, dissociative electron attachment (DA) will probe excited anion repulsive states in the electron–molecule scattering continuum. The effect of the strong electron–dipole interaction manifests as an asymmetry in the angular dependence of the negative-ion fragment, as shown experimentally from H^-/HF [7] and from our early Na^- results in the sodium halides [12,13]. Teillet-Billy and Gauyacq [14] have then extended the DA differential cross-section theory of O'Malley and Taylor [15] to include the effect of the long-range dipolar field of the target molecule. In our work on the alkali halides NaF, NaCl, and NaBr, we have used the

*Corresponding author. E-mail: j.p.tiesel@yosemite.ups-tlse.fr

Dedicated to Professor Aleksandar Stamatovic on the occasion of his 60th birthday.

PII S1387-3806(00)00291-8

angular dependence fits to the theory together with ion kinetic energy measurements in an attempt to determine the symmetry of the anion states involved in the DA processes.

2. Experimental

2.1. Spectrometers

Dissociative electron attachment in sodium halides has been studied with two different crossed-beam spectrometers. The magnetic spectrometer (MS) is used to measure the ion-yield spectra and calibrate the energy of the DA processes. Kinetic energy and angular distributions are then obtained in the electrostatic spectrometer (ES), first to distinguish between DA from the monomer and the dimer and then to access the spectroscopy of the dissociative NaX^- states.

In the magnetic spectrometer [16], the electron beam from a thoria-coated iridium filament is energy selected by a trochoïdal monochromator [17] and crosses the molecular beam effusing from a radiation-heated Knudsen oven. The negative ions are extracted at ~90° from the two beams by a small electric field and then mass analyzed by a 60° magnetic sector. The electrostatic spectrometer has been described in detail [18,19]. Briefly, the electron beam is energy selected in a 127° cylindrical filter and crosses the molecular beam issuing from a two-stage oven fitted with a 1-mm diameter exit canal 14 mm in length. The scattered electrons and negative ions coming from the collision zone are energy analyzed in a second 127° electrostatic filter that can rotate from 30° to 145° with respect to the incident electron beam. After energy analysis, ions and electrons of the same kinetic energy E_R are separated in a quadrupole mass filter and the ions are mass analyzed.

The oven temperatures are monitored with chromel-alumel thermocouples and set at ~1000 K, which corresponds to a NaCl vapor pressure inside the oven in the 10^{-2}torr-range [20]. In the MS, the oven exit hole is at 45 mm from the collision center and a shutter can stop the molecular beam to check if some species are coming from outside the oven. Electron currents are typically ~100 nA at an energy resolution of 150–200 meV; the Na^- count rate was then ~100 ions/s, with a draw-out field of a few tenths volt per centimeter. In the ES, the oven exit could be set at a distance as close as 2 mm from the collision center. With electron currents of 30 nA at a resolution of 120 meV, the Na^- count rate was also ~100 s^{-1} at a measurement angle of 90°. The molecular beam is then condensed on a cold finger at 2 cm above the collision center. The exit section of the two-stage oven can be slightly overheated to prevent clogging of the channel and to decrease the dimer production [20]. The heating wires are winded to cancel out the magnetic field [21], and indeed, no effect on the electrons was observed when operating the oven.

2.2. Modes of operation and energy-scale calibrations

In a dissociative attachment process, an incident electron of energy E_i is captured by the molecule to yield a negative ion and a neutral fragment as reaction products. The ion kinetic energy is given by the relation

$$E_R = (1 - \beta)(E_i - D_0 + EA - E^*), \quad (1)$$

where β is the ratio of the ion mass to that of the molecule, D_0 the dissociation energy to the products in their ground state, EA the electron affinity for the negative ion, and E^* the internal excitation energy deposited in the fragments.

Different modes of operation have been used in the electrostatic spectrometer and yield differential measurements at a fixed angle with respect to the incident electron beam in the plane perpendicular to the molecular beam. In the ion-energy mode, the incident electron energy is kept constant and the analyzer is swept to give the ion kinetic energy distribution. For a diatomic molecule, each peak in the ion-energy spectrum will then correspond to a different dissociation limit. A constant ion-energy spectrum is obtained by collecting ions of a fixed energy E_R while sweeping the incident energy E_i. In an ion-yield

spectrum, the ratio E_R to E_i is kept equal to $(1-\beta)$, and this mode gives the differential cross section (DCS) for a well-defined process as a function of electron energy.

In the magnetic spectrometer, the ions formed at ~90° of the electron and molecular beams are collected without kinetic energy analysis and the ion signal is recorded while sweeping the incident energy. The ions formed from the sodium halide beams show little variation of E_R through the dissociative energy range, and thus, there should be very little kinetic energy discrimination as a function of E_i. The ion-yield curves from the magnetic spectrometer can then be compared with the DCS at 90°, measured in the electrostatic spectrometer.

The electron energy scale is calibrated in the magnetic spectrometer with the vertical onset of O^-/CO at 9.62 eV [22]. A small amount of CO is flowed inside the collision chamber together with the sodium halide beam. The onset energy is assigned to the point of steepest rise in the experimental O^- curve, and this energy scale then corresponds to the most probable electron energy. The absolute peak energies are estimated within ±0.15 eV. As the onsets of the processes in NaX are not vertical, the determination of the appearance potentials is less straightforward. They are measured at an energy midway between the linearly extrapolated threshold, corresponding to the average energy of the electron beam and the energy at which the linear behavior of the cross-section leading edge is well-established [22]. The error limits (−0.15, +0.25 eV) take into account a probable underestimation of the threshold [23].

In the electrostatic spectrometer, the peak energies determined with the magnetic set-up are used for the calibration of the selector. The analyzer is calibrated by setting the incident energy at the Na^- peak and measuring the scattered electrons' energy-loss spectrum. The energy at the peak of the elastically scattered electrons is then $E_R = E_i$.

2.3. Ion angular distributions

Angular distributions are obtained by measuring the ion intensity as a function of the collection angle θ from 30° to 145° at constant energies E_i and E_R set by relation (1). Measurements are made relative to 90° and in series of three to minimize the effect of slow variations in the molecular beam density.

A number of effects can distort experimental angular distributions: thermal motion (translational and rotational) of the target molecule, momentum transfer, and collision region. The effects of the thermal motion and of the molecular recoil caused by momentum transfer have been discussed in detail for H_2 by Tronc et al. [24]. The effect of the translational velocity component in the direction of the molecular axis is to broaden the ion kinetic energy distribution [25]. The variation of this distribution width with the observation angle, as well as the momentum transfer, can cause an asymmetry in the angular dependence. However their influence was found to be small in H_2 if the ion intensity were measured for each angle at the distribution maximum [24]. We have used the same procedure in the angular measurements of Na^-. In contrast, translational motion in the direction perpendicular to the molecular axis, as well as rotation, can contribute to a loss of anisotropy in the angular distribution (see section 5.2). The kinetic energy of the molecules in the plane of analysis is difficult to know. Inside the oven, the gas is at equilibrium and its velocity given by a Maxwell-Boltzmann distribution. In an effusive beam, this distribution is assumed to be kept with, in the case of a planar aperture, a cosine law giving the fraction of molecules having a transverse velocity ν_T. The oven in the electrostatic spectrometer has an exit canal with a length-to-diameter ratio of 14, and the distribution should be more peaked in the forward direction than the cosine distribution. From a thin hole to our canal of the same diameter, the directivity, defined as the ratio of the flux around axis to the total emitted flux, is improved by a factor of 10 [26]. Apart from the improvement in the transverse speed distribution, a forward beam also has an effect on the angular variation of the useful volume of collision defined by the incident electron beam, the molecular beam, and the acceptance cone of the analyzer. When the molecular beam diameter is much larger than the collision zone determined by the electron beam, the angular measurements must be corrected by $\sin\theta$. In our experiment the correction

Table 1
Atomic and molecular negative-ion processes in sodium chloride

Ion	Onset (eV)	Peak (eV)	FWHM (eV)	Remark
Na^-	3.77	4.22	0.60	Present (3.68, 3.79 eV)[a]
	5.22	5.58		Present
	4.04			[27]
Cl^-	4.55	5.20	0.78	Present
	2.90			[27]
$NaCl^-$	5.00	5.67	0.72	Present
	5.08			[27]
Na_2Cl^-	4.75	5.38	0.76	Present
	4.76			[27]

[a] Thermochemical thresholds of DA into $Na^- + Cl^2P$.

should be smaller on account of the better directivity and the short distance between the exit and the interaction region.

3. Sodium chloride

Dissociative electron attachment processes in a sodium chloride beam are observed leading to the formation of Na^-, Cl^-, $NaCl^-$, and Na_2Cl^- ions. These processes have been energy calibrated in the magnetic spectrometer and can be compared to the previous data of Ebinghaus [27]. Studies completed in the electrostatic spectrometer have shown that some of the processes yielding atomic ions arise in fact from attachment to the dimer molecule. The angular behavior of the Na^-/NaCl differential cross section has also been measured.

3.1. The Na^- processes

The ion-yield curve obtained at ~90° in the MS shows two peaks at 4.3 and 5.6 eV (Table 1). The ES enables us to separate ions of the same species formed through different dissociation channels by tuning E_R to a selected dissociation limit. In the Na^-/NaCl ion-yield curve at 90° (Fig. 1), the high-energy process is no more observed and thus does not arise from a $NaCl^-$ state correlated to the dissociation products $Na^-{}^1S$ and Cl^2P. We then assign this process to dissociative attachment in the dimer $(NaCl)_2$, the dimer population in a sodium chloride vapor being as high as 25% at 920 K [20].

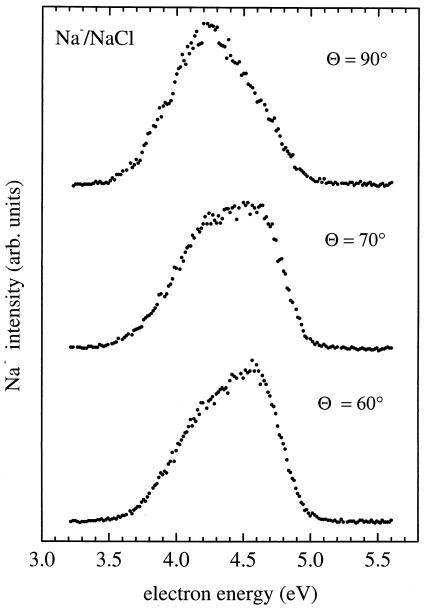

Fig. 1. Na^-/NaCl ion-yield curves at three scattering angles.

Also shown in Fig. 1 are the Na^- ion-yield curves at the observation angles of 70° and 60°. The instrumental resolution is not good enough to separate the Na^- ions associated with the $Cl^2P_{3/2}$ or $Cl^2P_{1/2}$ fine structure states. The spin-orbit splitting in Cl^2P is 109 meV, which would give a kinetic energy spacing of 66 meV between the two groups of ions, compared with a total spectrometer resolution of 200 meV as determined from the elastic electron peak. The DCS shape changes with angle as the maximum shifts from 4.2 eV at 90° to 4.6 eV at 60°. At the intermediate angle of 70°, a double maximum is apparent, suggesting that two processes with different angular dependence contribute to the Na^- formation in the electron energy range 3.8–5 eV. De facto, the ion angular distributions (Fig. 2) have quite a different shape at electron energies selected either on the low-energy side or on the high-energy side of the Na^- cross section. The angular distribution at $E_i = 4.08$ eV peaks near 110°, while at $E_i = 4.78$ eV it is minimum at this angle.

3.2. Cl^- formation

A single Cl^- process is observed (insert in Fig. 3), and the energies at onset and peak are reported in

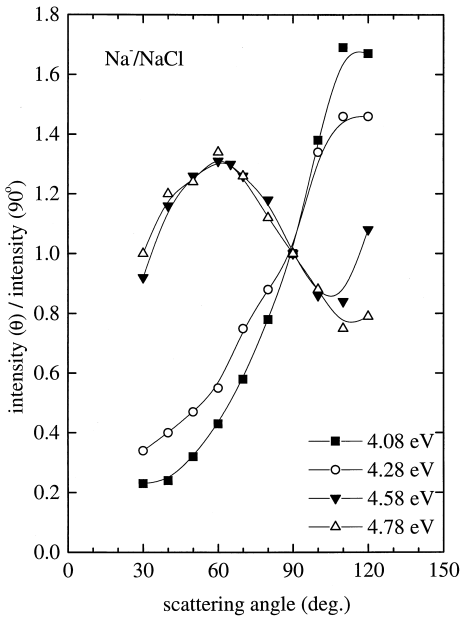

Fig. 2. Na^-/NaCl angular distributions at four electron energies: 4.08, 4.28, 4.58, and 4.78 eV. The solid lines are drawn to guide the eye through the experimental data.

Table 1. We have not observed any Cl^- formation between 0 and 4.5 eV electron energy, in disagreement with the observation of a low-energy process by Ebinghaus [27]. In Fig. 3 the ion-energy spectra of Cl^- at E_i = 4.95 eV and of Na^- at E_i = 4.20 eV are also shown. The shape of the Na^- distribution is symmetrical, contrary to the high-energy tail and the larger width of the Cl^- distribution. The FWHM for Na^- is ~300 meV, which is consistent with the main contribution from thermal broadening. The Doppler FWHM is given [24] by

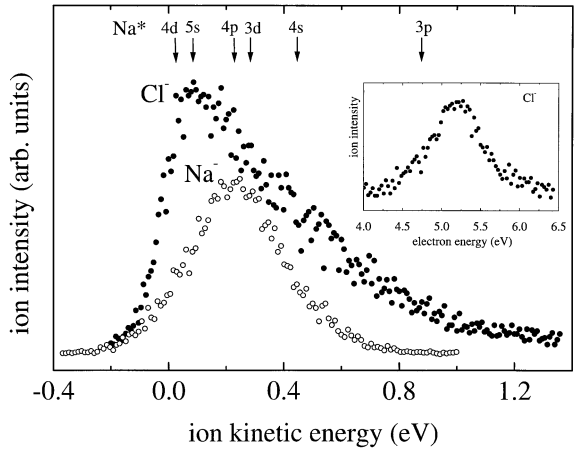

Fig. 3. Ion kinetic energy spectra of Cl^- at E_i = 4.95 eV (solid circles) and Na^- at E_i = 4.2 eV (open circles) from sodium chloride at a scattering angle of 90°. The Cl^- ion yield (magnetic spectrometer) is shown in the insert.

$$W_{1/2} = (11\beta kTE_R)^{1/2}, \quad (2)$$

where k is the Boltzmann constant and T is the translational temperature in the plane of analysis. This expression is strictly valid for the integrated distribution over all angles, but if we assume $W_{1/2}$ to be 300 meV, the transverse temperature can be roughly estimated at 625 K.

The Cl^- ion-kinetic spectra are peaked near zero energy over the whole cross section, in contrast to the Na^- spectra, where the maximum shifts with E_i according to relation (1). The usual interpretation of such a behavior is that most of the excess energy ($E_i - D_0$ + EA) is deposited as internal energy E^* in the neutral fragment associated with Cl^-. In a diatomic fragmentation, E^* would be purely electronic, while in a polyatomic fragmentation it can appear as vibrational and/or rotational energy. If the fragment is a sodium atom, there exists a large number of excited states between 2.102 eV and the ionization limit at 5.138 eV; we have indicated in Fig. 3 the positions of the Na excited states that could yield Cl^- kinetic energies between 0 and 1.3 eV. The Cl^- energy spectrum could then be a sum of overlapping spectra, each corresponding to a discrete excitation of Na. As the maximum stays close to 0 when the incident energy is increased, this implies that the formation of the highest Na excited state should always be the most probable. Different $NaCl^-$-resonant states would then have to be involved over the Cl^--formation energy range.

From the dimer presence in the molecular beam, it is more plausible to attribute Cl^- formation to dissociative attachment in $(NaCl)_2$, where not only electronic but also vibrational/rotational energy disposal in a molecular fragment may happen. The neutral fragments associated with Cl^- could be either NaCl and Na (case a) or Na_2Cl (case b). The available energy is calculated from the dissociation energies D_0

of Na_2Cl_2 [28], Na_2Cl [29], and NaCl [30] and from the electron affinity of Cl [31]. About 2.3 eV of excess energy could be deposited in the neutral fragments in case a and 3.1 eV in case b. The Na 3p excited states are energetically accessible but not the first excited NaCl state, as shown by the optical absorption threshold at ~4 eV, close to the minimum energy of this state [32]. The excited states of Na_2Cl are unknown, so a large number of electronically excited states cannot be invoked to explain the behavior of the Cl^- spectra. Rovibrational energy disposal in the molecular fragments is then the most likely process. The attribution of Cl^- formation to DA in the dimer is further supported by studies in NaF and NaBr where no halogen ions have been observed when overheating the exit stage of the oven.

3.3. Molecular ions

The onset and peak energies of the $NaCl^-$ and Na_2Cl^- formation processes are listed in Table 1, in good agreement with previous results [27]. The most likely process is DA to the dimer molecule, as the abundance of the trimer in a sodium chloride vapor is negligible [33]. The ion-kinetic energy spectra are shown in Fig. 4; the Na_2Cl^- and $NaCl^-$ distributions are peaked at zero energy and have an asymmetric shape similar to that observed for Cl^-. The energetics of the Na_2Cl^- process is not known. From D_0 (Na_2Cl-Cl) and the onset of Na_2Cl^-, only a lowest value of EA (Na_2Cl) can be determined at 0.95 eV. In the $NaCl^-/Na_2Cl_2$ process, the dissociation energy is ~2.24 eV [28] and the adiabatic EA (NaCl) is 0.727 eV [6]. An excess energy of ~4.2 eV is then transferred either into electronic excitation of the neutral NaCl fragment, into rovibrational excitation of the two molecular fragments, or into dissociation of the NaCl $^2\Sigma$ ground state, which needs an energy of 4.23 eV [30].

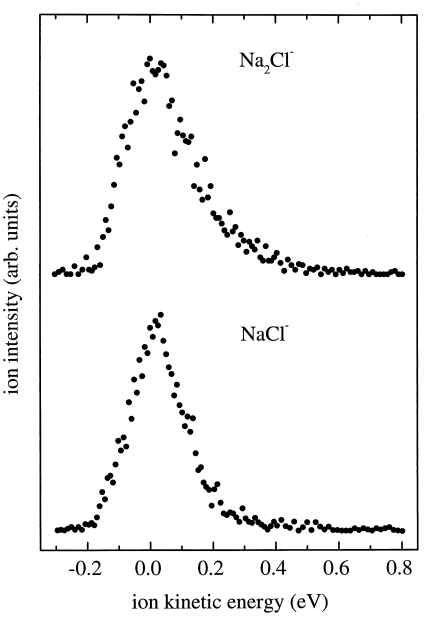

Fig. 4. Ion kinetic energy spectra of $NaCl^-$ at E_i = 5.67 eV and Na_2Cl^- at E_i = 5.38 eV from sodium chloride at a scattering angle of 90°.

4. Sodium fluoride, sodium bromide, sodium iodide

The dissociative attachment processes in sodium fluoride, bromide, and iodide observed in the magnetic spectrometer are listed in Table 2. Sodium iodide has only been studied in the MS, and energies of the processes are given here for the record. Unlike the study in NaCl, we have overheated the oven exit stage in the electrostatic spectrometer in an attempt to lower the dimer density. Then some of the Na^- and all of the X^- processes are no longer observed, such as the high-energy Na^- peak and F^- in sodium fluoride. This suggests that these ions (Table 2) are formed by DA in $(NaX)_2$ issuing from the single-stage oven while the dimers are dissociated in the two-stage oven.

The formation of Na^- in NaBr is of great interest as the spin-orbit splitting of Br^2P is large enough to study in the ES the processes leading to Na^- + $Br^2P_{3/2}$ and Na^- + $Br^2P_{1/2}$ (Fig. 5). There is one process correlated to the $Br^2P_{1/2}$ limit unlike DA in HBr [14], where two processes are observed, one of them arising from the coupling of the $^2\Sigma_{1/2}$ with the $^2\Pi_{1/2}$ state. Two processes are observed in the $Br^2P_{3/2}$ dissociation channel. The peak energies are quite different, suggesting that three resonant states are involved in the dissociative attachment. However, as

Table 2
Atomic and molecular negative-ion processes in sodium fluoride, sodium bromide and sodium iodide

Ion	Onset Energy (eV)		Peak (eV)	
	Present	[27]	Present	Comment
Na^-/NaF	4.55	4.66	5.1	(4.38, 4.43 eV)[a]
	6.25	6.3	6.75	b
F^-	4.7	2.55	5.25	b
	5.5	5.25	6.25	b
NaF^-	6.3	6.3	7.0	c
Na_2F^-	5.75	5.85	6.65	c
Na^-/NaBr	3.3	3.36	3.75	(3.21 eV)[a]
	4.25		4.45	(3.67 eV)[a]
	4.85		5.1	b
Br^-	3.65	3.75	4.1	b
	4.15		4.6	b
			5.5	b
$NaBr^-$	4.35	4.38	4.85	c
Na_2Br^-	4.05	4.08	4.6	c
Na^-/Na	2.65	2.84	3.1	c (2.76 eV)[a]
			4.2	c (3.70 eV)[a]
I^-	2.1		2.55	c
	3.15	3.25	3.8	c
			4.6	c
NaI^-	3.4	3.54	4.0	c
Na_2I^-	3.2	3.26	3.7	c
Error	+0.25 −0.15	±0.2	±0.15	

[a] Thermochemical thresholds: the lowest value corresponds to the dissociation into $Na^- + X^2P_{3/2}$, the other into $Na^- + X^2P_{1/2}$.
[b] Not observed in the electrostatic spectrometer.
[c] Only studied in the magnetic spectrometer.

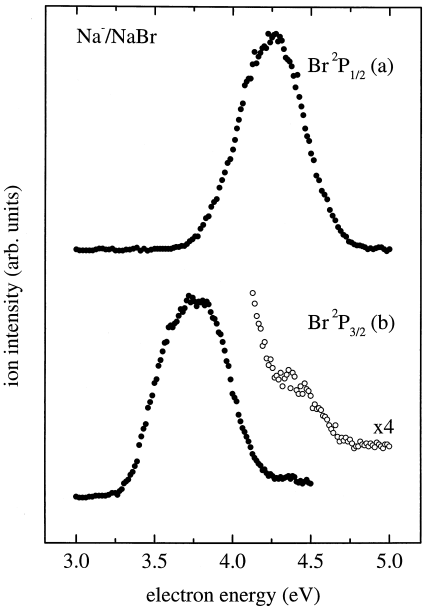

Fig. 5. Na^-/NaBr ion-yield curves at a scattering angle of 47°: (*a*) dissociation to $Br^2P_{1/2}$; (*b*) dissociation to $Br^2P_{3/2}$.

discussed below (see section 5.3), the attribution of the low-intensity peak ~4.5 eV to DA in the monomer is doubtful. The onsets of the two main processes are very close to the thermochemical thresholds, which implies that the potential energy curves of the molecular anion states must be flat at large R or even have a shallow minimum.

The angular dependence of the Na^-/NaBr processes, normalized with respect to the 90° scattering angle, are shown at four different energies in Fig. 6. These angular distributions reflect the variation of the relative DCS $d\sigma/d\Omega$. Along the cross section for each dissociation channel, there is no drastic change of the general shape, unlike our measurements in Na^-/NaCl (Fig. 2) or Na^-/NaF (Fig. 7). For these ions, the dissociation channels to X^2P are studied as a whole, resulting in a mixture of all the involved resonant states. A common feature of all the Na^-/NaX angular distributions is a strong asymmetry with respect to $\theta = 90°$, which reflects the preferential attachment of the electron to the Na^+ side of the polar molecule [14].

5. Symmetry of the resonant dissociative NaX^- states

Two molecular states of Σ and Π symmetry are correlated to the dissociation limit $Na^-{}^1S + X^2P$. These states are Feshbach resonances with electron configurations $\pi^4\sigma^1\sigma'^2$ and $\pi^3\sigma^2\sigma'^2$, where the LUMO σ' is filled by one excited valence electron and the attaching incident electron. The coupling by the spin-orbit interaction splits them into three states, of which two are defined by the quantum number $\Omega = 1/2$ and one with $\Omega = 3/2$. The attachment to the $\Omega = 3/2$ state and then the Na^- angular distribution (see following) should be both typical of a state of Π symmetry and a sum of the contribution of Σ and Π symmetries for the two $\Omega = 1/2$ states.

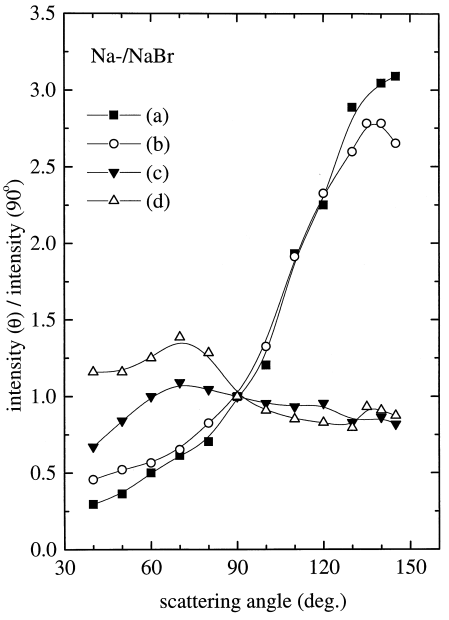

Fig. 6. Experimental angular distributions of Na^-/NaBr: dissociation to $Br^2P_{3/2}$ at $E_i = 3.77$ eV (*a*) and 3.97 eV (*b*); dissociation to $Br^2P_{1/2}$ at $E_i = 4.277$ eV (*c*) and 4.57 eV (*d*). The solid lines are drawn to guide the eye through the experimental data.

5.1. DA differential cross sections with a dipolar field

Assuming that the dissociation of the resonant state is fast compared to the rotation of this intermediate anion, the DA differential cross section at an angle θ between the incident electron beam and the internuclear axis is then related to the probability of attachment to the neutral molecule at θ. This probability depends on the electronic coupling element V between the resonant state and the continuous wave function of the entrance channel (electron + molecule). Assuming that the interaction potential is of spherical symmetry, the incident electron plane wave is developed in spherical harmonics and the angular dependence of V is then contained in $Y_{lm}(\theta)$. A theoretical treatment has been given by O'Malley and Taylor [15] based on the formalism of O'Malley [34]. Within the slow rotation approximation, the angular part of the DCS $d\sigma(\theta,k_i)/d\Omega$ is expressed as a squared modulus of a sum of spherical harmonics $Y_{lm}(\Omega)$ over l from m to ∞, k_i being the incident electron wave number. From

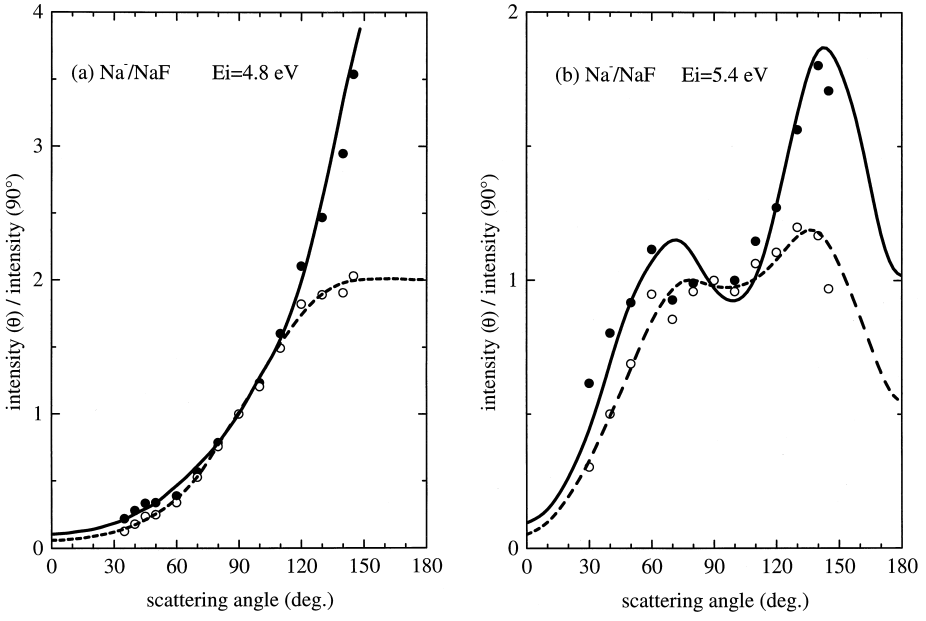

Fig. 7. Angular distributions (corrected) of Na^-/NaF: (*a*) $E_i = 4.8$ eV: filled circles, experimental data; solid line, theory, Φ_0^0 and Φ_1^0 modes; open circles, corrected experimental data; dotted line, theory, Φ_0^0 and Φ_1^0 modes. (*b*) $E_i = 5.4$ eV: solid circles, experimental data; solid line theory: Φ_1^1 and Φ_2^1 modes; open circles, corrected experimental data; dotted line, theory, Φ_1^1 and Φ_2^1 modes.

the axial momentum conservation, m is $|\Lambda_r - \Lambda_t|$, where Λ_r and Λ_t are the resonance and target axial angular momenta. For heteronuclear diatomics, all the $l \geq m$ values are allowed, but for homonuclear molecules, l will be either even or odd depending on the parity, same or opposite, of the initial and resonant states. In homonuclear molecules, the fragment-ion angular distribution will then always be symetrical with respect to 90°. In heteronuclear molecules, this is also the case when only one incident electron partial wave is involved, but the contribution of several partial waves may eventually produce distributions with forward-backward asymmetry, as observed in O^-/CO [35] and in H^-/HI [36]. When looking to the hydrogen halides and sodium halides series, the asymmetry is not present in H^-/HBr ($\mu = 0.8$ D) [17] and H^-/HCl (1.08 D) [37] but appears in H^-/HF (1.82 D) [9] and becomes more pronounced in the sodium halides (8.1–9.1 D). A slight asymmetry is even present in the H^- distributions from the triatomic molecules H_2S (0.97 D) [38] and H_2O (1.85 D) [39].

The theory of O'Malley and Taylor [15] does not take into account the dipolar interaction in the attachment, as it is assumed that the electron-molecule interaction is spherically symmetric at large electron–molecule distances. Teillet-Billy and Gauyacq [14] have extended the theory to polar and highly polar molecules by introducing the anisotropic interaction $2\mu \cos\theta r^{-2}$ for a pure point dipole. The spherical harmonics Y_{lm} are then replaced by the dipolar angular eigenmodes Φ_n^m, expanded as a sum of $A_{lm}Y_{lm}(\Omega)$, where the coefficients A_{lm} are dependent on μ. The selection rule $m = |\Lambda_r - \Lambda_t|$ still applies. Finally, the angular part of the DCS will depend on the fixed orientation of the molecule during dissociation only through Φ_n^m, and its expression is $[d\sigma/d\Omega \propto |\Sigma^{\infty}_{n=m} a_n^m \Phi_n^m|^2$. This theory has been proved successful by analyzing the angular distribution of the H^-/HF process ~9.5 eV with the Φ_1^1 mode alone; the H^- resonant state is then unambiguously of $^2\Pi$ symmetry as $\Lambda_r = m = 1$ [11].

From the comparison between the theoretical and experimentally measured angular distributions of the Na^- fragment, we expect to be able to determine the symmetry of the dissociating NaX^- state. We assume a given symmetry Σ or Π for the NaX^- state. In a few cases, we have also considered the possibility that two dissociative states of different symmetry contribute to the process. For a single symmetry, it is assumed that only two modes are necessary to describe the attachment angular dependence, with the amplitude of each mode and their relative phases as parameters. For the analysis with two contributing symmetries, each was described with one single mode and two parameters were used, as there is no interference between the spin-orbit coupled states. The theoretical description given here describes the ion angular behavior in a dissociative electron attachment process on a target molecule supposed to be fixed in space and not to rotate. In the present experimental operating conditions, the kinetic and internal energies of molecules at the oven temperature are not negligible compared with the dissociation energy, and this induces a loss of anisotropy in the angular distribution [14]. We have included these corrections in the theoretical approach.

5.2. Na^-/NaF, Na^-/NaCl angular distributions

The angular distributions of Na^-/NaF are shown at two energies in Fig. 7. Even when the maximum correction in $\sin\theta$ is applied to the experimental data (see section 2.3), the strong asymmetry with respect to 90° is still there. The main effect arises from the kinetic and rotational energies of the target molecule effusing from the oven. The loss of anisotropy caused by the translation increases with the temperature and inversely decreases with the fragment-ion kinetic energy. As for the rotational effect, the average angle of rotation during the dissociation to Na^- is ~20° in a beam of NaCl at 1000 K [14]. We have taken into account the averaging effect caused by both the target translation and the rotation on the theoretical angular distribution by an angle convolution procedure with an estimated convolution width of 40°. This angle convolution of 40° width has been applied to all the theoretical distributions. We thus compare the experimental distributions with the convoluted theoretical angular distributions after adjustment of the parameters of the theoretical description. We have ascer-

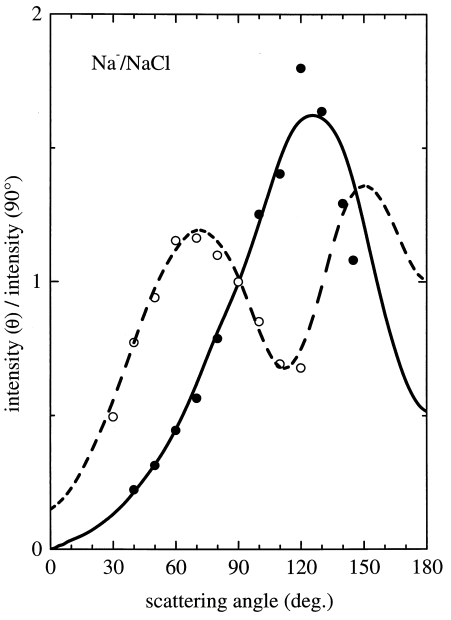

Fig. 8. Angular distributions (corrected) of Na^-/NaCl: E_i = 4.11 eV: filled circles, experimental data; solid line, theory, Φ_1^1 and Φ_2^1 modes. E_i = 4.78 eV: open circles, corrected experimental data; dotted lines, theory, Φ_2^1 and Φ_3^1 modes.

tained that convolution with a width as large as 60° does not change the data analysis conclusions.

In Na^- from NaF and NaCl (Fig. 8), it is found that every experimental distribution can be fitted with a Π symmetry within the experimental errors. The correction in $\sin\theta$ for the collision volume improves the agreement between the theoretical and experimental distributions (Fig. 7). For most of the energies, the two modes involved are Φ_1^1 and Φ_2^1, although in Na^-/NaCl the quality of the fit improves on the high-energy side when Φ_2^1 and Φ_3^1 are used. The angular distributions can also be fitted with a combination of the Φ_0^0 and Φ_1^0 modes (Σ symmetry), but the quality of the analysis is generally not as good as with a Π symmetry, except at energies close to the Na^- onsets in which the Σ modes seem dominant. No satisfactory agreement has been obtained when combining two modes of different symmetries. More modes are probably needed, but the large number of parameters involved has precluded such an extended analysis.

5.3. Na^-/NaBr angular distributions

In NaBr, the two dissociative attachment channels have been studied separately. The angular distributions of Na^- correlated to $Br^2P_{1/2}$ decrease at large angles (Fig. 9a) and are best fitted with modes of Π symmetry, even at low energy. In the $Br^2P_{3/2}$ channel, the Π symmetry dominates over the process (Fig. 9a) with a possible contribution of Σ character at low energy (Fig. 9b). The nonobservation of a significant Σ symmetry, even in the upper state $2(\Omega = 1/2)$ could be caused by a weak attachment probability in the Σ state.

The small structure ~4.5 eV in the Na^- ion yield correlated to $Br^2P_{3/2}$ (Fig. 6b) could arise from the $2(\Omega = 1/2)$ state, either through a nonadiabatic transition as observed in H^-/HBr or by incomplete experimental filtering. However, dissociative attachment to the dimer fraction remaining in the beam cannot be excluded.

6. Conclusion

We have determined that no halogen ion X^- are formed by dissociative attachment to the NaX molecules. The observed X^- processes are attributed to DA in the sodium halides dimer molecules. These ionic clusters are also probably responsible for the formation of the NaX^- and Na_2X^- molecular ions. Aside from the positive electron affinity of $(NaCl)_2$ [40] resulting in a ground anion state that is bound, the excited anion states are unknown. For NaCl, a resonance has been observed in the electron + NaCl continuum in a photodetachment experiment [41] and attributed to the $A^2\Pi$ state of NaX^- correlated to Na(3p) + Cl^-. Calculations in LiF have shown that the excited $A^2\Pi$ and $B^2\Sigma$ anion states are either attractive in the continuum [42] or even bound with respect to the neutral ground state [43]. These states could then not give rise to X^- formation, in agreement with our results.

The Na^- processes in NaF, NaCl, and NaBr show a strong asymmetry toward large angles in their angular distributions, which can be interpreted as favored electron attachment to the electropositive

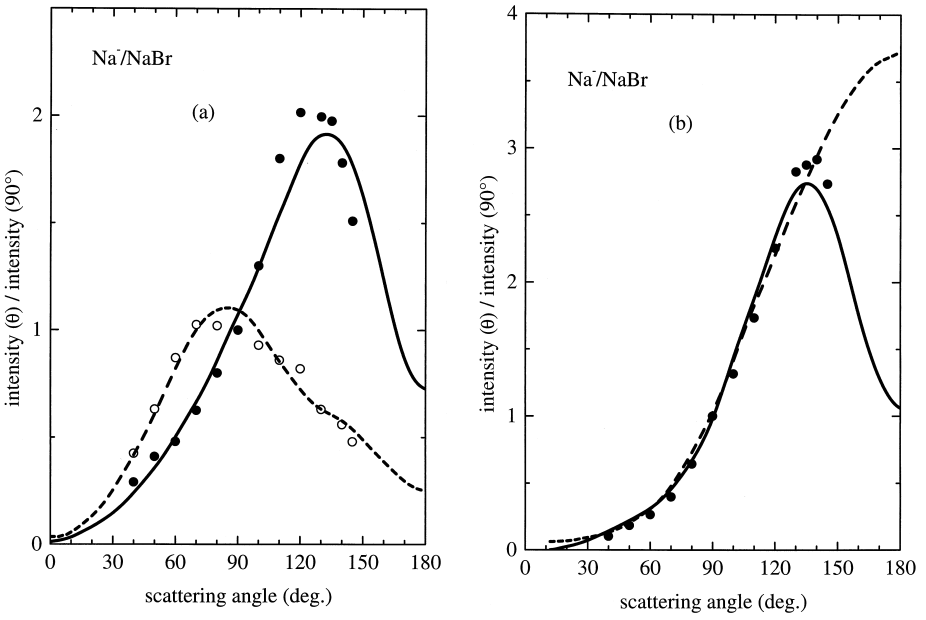

Fig. 9. Angular distributions (corrected) of Na^-/NaBr: (*a*) dissociation to $Br^2P_{1/2}$ at $E_i = 4.27$ eV: filled circles, experimental data; dotted lines, theory, Φ_1^1 and Φ_2^1 modes. Dissociation to $Br^2P_{3/2}$ at $E_i = 3.97$ eV: filled circles, experimental data; solid lines, theory, Φ_1^1 and Φ_2^1 modes. (*b*) Dissociation to $Br^2P_{3/2}$ at $E_i = 3.62$ eV: filled circles, experimental data; solid line, theory, Φ_1^1 and Φ_2^1 modes; dotted lines, theory, Φ_1^0 and Φ_2^0 modes.

atom of the highly polar molecule. We have analyzed these distributions in the frame of the theory of Teillet-Billy and Gauyacq. It seems that attachment mainly proceeds through the Π character of the anion states, while the Σ character only contributes near the onsets.

References

[1] J.-P. Ziesel, I. Nenner, G.J. Schulz, J. Chem. Phys. 62 (1975) 1943.
[2] K. Rohr, F. Linder, J. Phys. B 9 (1976) 2521.
[3] J.-P. Gauyacq, Dynamics of negative ions, World Scientific, Singapore, 1987.
[4] W. Domcke, Phys. Rep. 208 (1991) 97.
[5] M. Cizek, J. Horacek, A.-Ch. Sergenton, D. Popovic, M. Allan, W. Domcke, T. Leininger, F.X. Gadea, Phys. Rev. A, in press.
[6] T.M. Miller, D.G. Leopold, K.K. Murray, W.C. Lineberger, J. Chem. Phys. 85 (1986) 2368.
[7] J.L. Carlsten, J.R. Peterson, W.C. Lineberger, Chem. Phys. Lett. 37 (1976) 5.
[8] K.D. Jordan, W. Luken, J. Chem. Phys. 64 (1976) 2760.
[9] K.D. Jordan, Acc. Chem. Res. 12 (1979) 36.
[10] C. Desfrançois, H. Abdoul-Carine, J.-P. Schermann, Int. J. Mod. Phys. B 10 (1996) 1339.
[11] R. Abouaf, D. Teillet-Billy, R. Azria, and P. Girard, J. Phys. B 18 (1985) 3017.
[12] J.-P. Ziesel, Lecture Notes in Chemistry 35, Springer, Berlin, 1984, p. 39.
[13] R. Azria, Comments At. Mol. Phys. 15 (1984) 1.
[14] D. Teillet-Billy, J.-P. Gauyacq, J. Phys. B 17 (1984) 3329.
[15] T.F. O'Malley, H.S. Taylor, Phys. Rev. A 176 (1968) 207.
[16] J.-P. Ziesel, D. Teillet-Billy, L. Bouby, Chem. Phys. Lett. 123 (1986) 371.
[17] A. Stamatovic, G.J. Schulz, Rev. Sci. Instr. 41 (1970) 423.
[18] Y. Le Coat, R. Azria, M. Tronc, J. Phys. B 15 (1982) 1569.
[19] Y. Le Coat, L. Bouby, J.-P. Guillotin, J.-P. Ziesel, J. Phys. B 29 (1996) 545.
[20] R.C. Miller, P. Kusch, J. Chem. Phys. 25 (1960) 860.
[21] I.V. Hertel, K.J. Ross, J. Phys. E: Sci. Instrum. 2 (1969) 1245.
[22] P.J. Chantry, Phys. Rev. 172 (1968) 125.
[23] P.J. Chantry, J. Chem. Phys. 65 (1976) 4414.
[24] M. Tronc, F. Fiquet-Fayard, C. Schermann, R.I. Hall, J. Phys. B 10 (1977) 305.
[25] P.J. Chantry, G.J. Schulz, Phys. Rev. 156 (1967) 134.
[26] M.A.D. Fluendy, K.P. Lawley, Chemical Applications of Molecular Beam Scattering, Chapman and Hall, London, 1973.
[27] H. Ebinghaus, Z. Naturforsch. 19A (1964) 727.
[28] G.M. Rothberg, J. Chem. Phys. 34 (1961) 2069.
[29] M.M. Kappes, P. Radi, M. Schär, E. Schumacher, Chem. Phys. Lett 113 (1985) 243.
[30] T. Min, R. Su, S.J. Riley, J. Chem. Phys. 72 (1980) 6632.

[31] H. Hotop, W.C. Lineberger, J. Phys. Chem. Ref. Data 14 (1985) 731.
[32] P. Davidovits, D.C. Broadhead, J. Chem. Phys 46 (1967) 2968.
[33] M. Blander, in: P. Davidovits and D.L. McFadden (Ed.), Alkali Halide Vapors: Structure Spectra and Reaction Dynamics, Chapter 1: The thermodynamic properties of alkali halide vapors. pp. 25–29, Academic Press, New York, 1979.
[34] T.F. O'Malley, Phys. Rev. 150 (1966) 14.
[35] R.I. Hall, I. Cadez, C. Schermann, M. Tronc, Phys. Rev. A 15 (1977) 599.
[36] Y. Le Coat, R. Azria, M. Tronc, J. Phys. B 18 (1985) 809.
[37] R. Azria, Y. Le Coat, D. Simon, M. Tronc, J. Phys. B 13 (1980) 1909.
[38] R. Azria, Y. Le Coat, G. Lefèvre, D. Simon, J. Phys. B 12 (1979) 679.
[39] R.I. Hall, S. Trajmar, J. Phys. B 7 (1974) L458.
[40] P. Xia, Naichang Yu, L.A. Bloomfield, Phys. Rev. B 47 (1993) 10040.
[41] S.E. Novick, P.L. Jones, T.J. Mulloney, W.C. Lineberger, J. Chem. Phys. 70 (1979) 2210.
[42] W.J. Stevens, J. Chem. Phys. 72 (1980) 1536.
[43] A.U. Hazi, J. Chem. Phys. 75 (1981) 4586.